Modal Engineering of Inductive Circuits to Achieve Rapid Settling Times

Josh Javor[1], Lawrence Barret, Matthias Imboden, Russel W. Giannetta, David K. Campbell, David J. Bishop, *Member, IEEE*

***Abstract*—Inductive circuits and devices are a ubiquitous and important design element in many applications such as magnetic drives, galvanometers, magnetic scanners, applying DC magnetic fields to systems, RF coils in NMR systems and vast array of other applications. They are widely used to generate both DC and AC magnetic fields. Many of these applications require a rapid step and settling time, turning the DC or AC magnetic field on and off quickly. The inductive response normally makes this a challenging thing to do. In this article we discuss open loop control algorithms for achieving rapid step and settling times in four general categories of applications: DC and AC systems where the system is either under or over damped. Each of these four categories requires a different algorithm which we describe here. We show the operation of these drive methods using Simulink and Simscape modeling tools, analytical solutions to the underlying differential equations and in experimental results using an inductive magnetic coil and a Hall sensor. Finally, we demonstrate application of these techniques to significantly reduce ringing in a standard NMR circuit. We intend this article to be practical with useful, easy to apply algorithms and helpful tuning tricks.**

***Index Terms*—open-loop controls, dead time, ringing, NMR, inductive sensors, modal engineering**

I. Introduction

Magnetic fields, both AC and DC, are generated for use in a vast array of applications. These include galvanometers and scanners [1]-[3], NMR systems [4]-[11], magnetic nanoparticle detection [12]-[13], permanent magnet actuation [14]-[15], magnetic latches, magnetic separation schemes, energy analysis for electron beams and many others. In a large subset of these applications, one wishes to turn the DC or AC magnetic field on and off quickly. However, the inductive response makes this difficult. In overdamped systems, the $\tau_D = \frac{L}{R}$ response time sets the time scale, and in underdamped systems, the Q limits the response time characterized by the settling time $\tau_Q = \frac{2\,Q}{\omega_0}$ (where L is the inductance, R the resistance, Q the quality factor and $\omega_0 = \frac{1}{\sqrt{LC}}$ the resonance frequency of the circuit). Closed loop systems using feedback can be used to mitigate these issues but these require a sensor, a PID controller and a feedback loop [16], adding cost and complexity.

Open loop control algorithms have the advantage of simplicity and are easy to implement with minimal overhead. Typically, they use complex voltage waveforms but modern, high-speed microprocessors make this increasingly easy. Open loop algorithms do require that the system be time invariant which is usually a good assumption for many applications. The algorithms discussed here assume one knows the underlying system dynamics in detail. By leveraging that understanding, one can apply drive signals that elicit the correct system response. In a sense, one doesn't fight the system but uses its response, in a coherent way, to get to the desired output.

We call this approach modal engineering, where one controllably adds and removes energy from the modes of the system, in a way that is coherent with its underlying dynamics. In a previous set of papers [1], [2], [14], [17], we have used

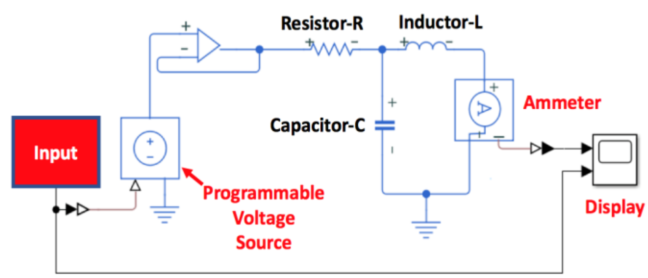

Fig. 1. Parallel LCR circuit via Simscape. This circuit configuration is used to demonstrate, both experimentally and in simulations, four cases of inductor drive applications: DC and AC in underdamped and overdamped cases. The system is driven by a voltage source and the coil response is collected by an ammeter in simulations and by a Hall sensor in experiments.

This work was supported by the NSF CELL-MET ERC award no. 1647837 and a SONY Faculty Innovation Award.

J. Javor is with the Department of Mechanical Engineering, Boston University, Boston, MA 02215 USA. (email: jjavor@bu.edu)
L. Barrett is with the Division of Materials Science and Engineering, Boston University, Boston, MA 02215 USA. (e-mail: blawrenc@bu.edu).
M. Imboden is with the STI-IMT LMTS, École Polytechnique Fédérale de Lausanne, 2002 Neuchâtel, Switzerland (e-mail: m.imboden@gmail.com).
R.W. Giannetta is with the Department of Physics, University of Illonois, Champaign, IL 61820, USA. (russg@illinois.edu)
D. K. Campbell is with the Division of Materials Science and Engineering, Department of Electrical and Computer Engineering, Department of Physics, Boston University, Boston, MA 02215 USA. (email: dkcampbe@bu.edu)
D. J. Bishop is with the Division of Material Science and Engineering, Department of Electrical and Computer Engineering, Department of Physics, Department of Mechanical Engineering and Department of Biomedical Engineering, Boston University, Boston, MA 02215 USA. (email: djb1@bu.edu). Josh Javor is the corresponding author.

these approaches to control the behavior of MEMS devices, improving the step-and-settle time in both galvanometer (DC) and scanner (AC) applications. In this paper, we apply these approaches to inductive systems used to generate DC and AC magnetic fields. Of course, the underlying principles are similar, but there are some subtle differences in how they are applied in inductive systems which we discuss here.

This work is organized based on four general categories of magnetic field application: DC underdamped, DC overdamped, AC underdamped, and AC overdamped. The algorithms in each category have some common traits but are different in each group. We essentially describe a recipe book with easy-to-implement algorithms and tuning tricks. Using the outlined techniques, we demonstrate and discuss the application of these algorithms to a nuclear magnetic resonance (NMR) circuit. Typical NMR systems use an underdamped, high-Q coil to generate the fast radiofrequency (RF) pulses needed to orient the atomic spins. Such systems remain plagued by the design tradeoff between measurement resolution and dead time. Less damping (higher Q) enables the largest magnetic field from the available RF power, but then one must wait for the coil to ring down before making a measurement, sacrificing faster relaxation information and higher signal-to-noise (SNR) data points. The algorithms discussed here allow one to have both the benefits of high-Q in terms of large resonant enhancements in the generated RF magnetic field and rapid on/off settling, typically in less than an RF period. We predict that such techniques will prove pivotal for NMR applications such as high resolution cryogenic systems [18], fast-relaxation solid samples [19], surface NMR systems for analyzing deep underground materials [4], low-field NMR [6], [10]-[11], and magnetic resonance imaging (MRI) systems, both stationary [5] and portable [20].

II. Background

The generalized circuit diagram for an inductor system is shown (Fig. 1). We are applying a voltage source to an inductor L, in parallel with a capacitor C, which are then in series with a resistor R. For most of what follows, we assume the coil resistance is zero. This does not change the behavior of the voltage drives to a significant extent. For our experimental and simulation results using a current drive (see *SI Appendix*, Fig. S2 and Fig. S4), we explicitly include it. There are other arrangements we could have chosen. For example, we could have chosen a series LCR system but with such a setup one cannot generate DC magnetic fields. We use this system because it can demonstrate all four operating regimes, DC and AC drives with coils that are under- or over- damped. The approaches are general and can be applied to other circuit configurations, albeit with different parameters.

The parallel LCR circuit is driven by a voltage source, and the ammeter measures the current flowing through the inductor. This is directly related to the generated magnetic field. In experimental results, we measure the generated AC or DC magnetic field with a Hall sensor. For this arrangement of resistor, capacitor and inductor, the resonant frequency and Q are:

$$f = \frac{1}{2\pi\sqrt{LC}} \qquad Q = R\sqrt{\frac{C}{L}} \tag{1}$$

TABLE I

Coil Parameters for Simulations and Experiments

Symbol	Parameter	Units	Underdamped Case	Overdamped Case
R	Resistance	Ohms	1000	10
L	Inductance	mH	10.31	10.31
C	Capacitance	μF	2.45	0
Q	Quality factor	-	15.437	0.015
f_0	Resonant Frequency	kHz	1	1

Coil parameters illustrated schematically in Fig. 1 are listed for two cases, used in simulations and matched in experiments.

We use four tools to discuss our algorithms. These are Simscape for circuit simulation, Simulink for transfer function analysis (ratio of voltage input to inductor current output), closed form analytical solutions of the relevant differential equations and, finally, low frequency experiments on an inductor, capacitor and resistor with the generated magnetic field measured with a Hall sensor that demonstrate all the algorithms. The circuit element parameters for the underdamped and overdamped case are shown in Table 1. Values are chosen such that simulation and experiment can be compared.

In what follows, we discuss the four relevant regimes of operation: DC underdamped (III), DC overdamped (IV), AC underdamped (V) and AC overdamped (VI). In the last section (VII), we present an analysis on a typical NMR drive circuit. Finally, we predominantly focus on voltage drives in simulations and experiments, but analysis of a current drive system (Fig. S2) and, separately, a control theory approach (Fig. S3 and S4) is included in the *SI Appendix*.

III. DC Magnetic Fields, Underdamped Circuit

In this section, we apply a DC voltage drive to an underdamped, high-Q circuit. Simscape is used to simulate the response of three different drives (Fig. 2). A normal step response is shown first (Fig. 2a), where the system rings for tens of periods (tens of milliseconds). The settling is improved by engineered, open loop drives. A “two-step” input is designed and results in settling in ~1/2 a period, or ~1/2 a millisecond (Fig. 2b). An “overdrive” input yields ~1/3 of a millisecond (Fig. 3c). The overdrive improves the step-and-settle time for this system by roughly a factor of 100.

The two-step applies the input to the system in two stages. In the first step, one applies just over one half of the final driving force. One waits for half of a (damped) period and then applies the final driving force. This response is discussed in detail in our previous work [1]. Briefly, the technique relies on the overshoot one sees in driving an underdamped (high-Q) system. When one applies a step input to an underdamped system, it overshoots close to twice the final resting position and then oscillates about that final resting position with a decreasing amplitude. For an underdamped system, at the first excursion, the system is at twice the final position and at the top of the peak. At one half a period, the velocity (slope of the position curve with time) is zero. The two-step exploits this response by applying one half of the force and then “catching” the system after one half a period with the second step. When one applies a step with half the force, after one half a period, the system is where it is supposed to be with zero velocity. The application of the second half of the force then creates a situation where it is intended to go, its velocity is zero (no kinetic energy) and the net force on it is zero. It stays there in a stable position and has been driven there in one half a period. The values of half the force for half the period are exact only for infinite-Q systems. For finite-Q, they can be modified below:

$$T_1 = \frac{T_0}{2\sqrt{1-\left(\frac{1}{2Q}\right)^2}} \qquad F_1 = F_0\left(1-\frac{1}{1+e^{\frac{\omega_0 T_1}{2Q}}}\right) \qquad (2)$$

where the first step consists of force F_1 applied for a time T_1. T_0 is the undamped system period, Q is the system quality factor, F_0 is the full force to be applied to the system and ω_0 is the undamped angular frequency. In the limit of $Q\rightarrow\infty$, the expressions in Eq (2) return the half period and half force condition. Typically, for Q>100, the infinite-Q limit values suffice for practical use.

To decrease ringing, one uses the restoring force of the resonator to slow the rate of change of the current (Fig. 2b and c). The current (object) is initially zero (at rest), it is ramped up (accelerated) for a period of time and then it is decelerated for a period of time, arriving at the new steady current (position) with no time variance (zero velocity) and balanced voltage (zero net force). In the overdrive method (Fig. 2c), one applies an accelerating voltage (force) for 1/6 of a period, removes the voltage (force) for 1/6 of a period and then reapplies it after 1/3 of a period (1/6 on and 1/6 off). Removing the voltage (force) after 1/6 of a period decelerates the system because of the restoring force. After 1/3 of a period, it arrives where desired with no changes in current (velocity) and balanced voltage (no net force). The timing of 1/6 period on and then 1/6 period off is exactly true for infinite-Q systems. For finite-Q systems, the timing needs to be modified accordingly [1].

In both the two-step and overdrive method, one has applied a unipolar Voltage (e.g. the applied force drives the system where desired and the decelerating force is the spring constant). In inductive systems, one can, in principle, apply both positive and negative voltages and then apply larger accelerating and decelerating forces and accomplish moving the system even more quickly. We have previously demonstrated this approach to create step-and-settle response times of second order systems in a little as 1/10 of a period [1]. If one has a drive available such that one can overvoltage the system both positively and negatively, one can switch DC magnetic fields as quickly as one wishes, limited only by the voltage overhead available in the drive system. For example, if one has 10X in voltage overhead, one can switch in ~1/10 of a period. With 5X voltage overhead, one can switch the system in ~1/5 of a period. And, using two-step or overdrive with no voltage overhead, one can switch in 1/2 or 1/3 of a period, respectively. Amplifier compliance can often be a limitation, and so the two-step or unipolar overdrive are convenient approaches because they require no voltage overhead, merely timing.

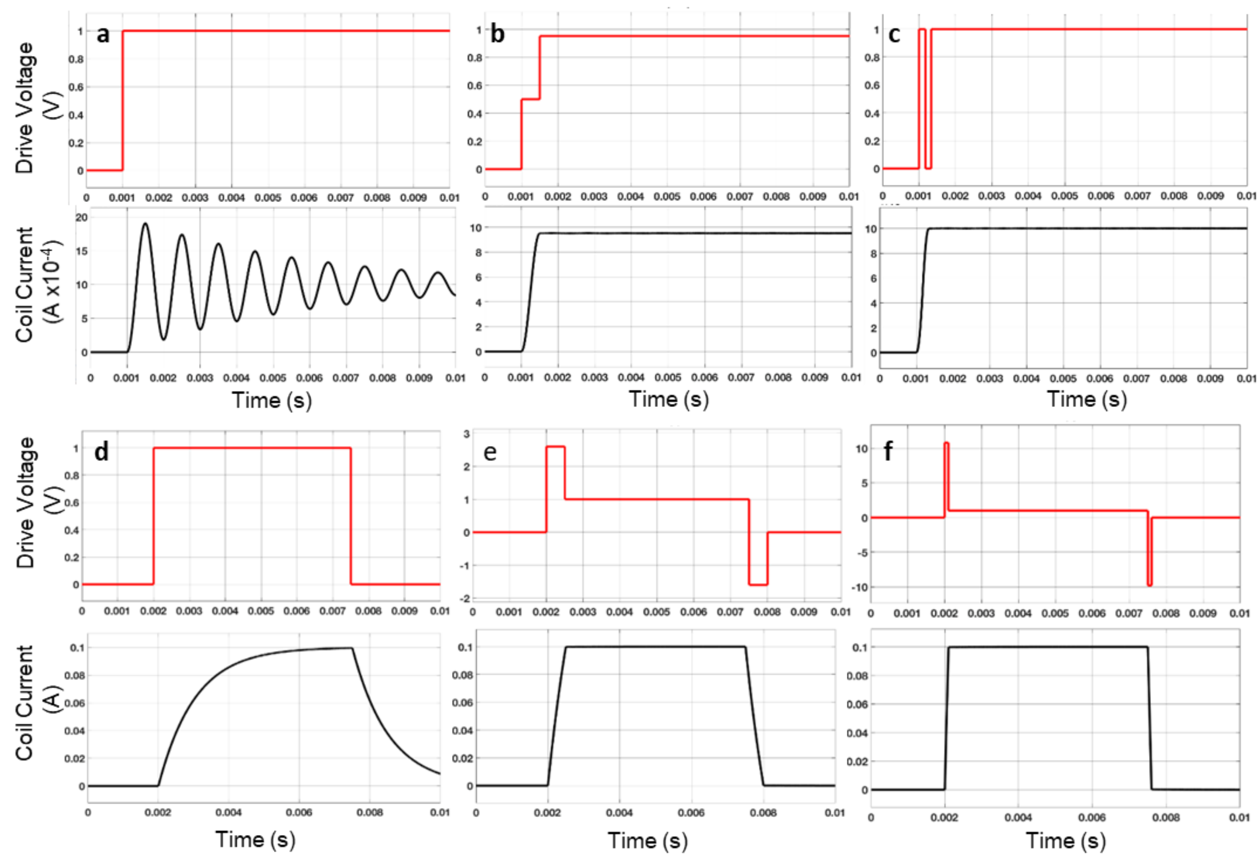

Fig. 2. DC Magnetic Field Simulations. Shown are Simscape simulations of the parallel LCR circuit shown in Fig. 1, for underdamped (a-c) and overdamped (d-f) parameters in Table 1 and a DC drive (voltage drives are red/top and the inductor currents are black/bottom. The underdamped case are responses to (a) a normal step, (b) two-step drive, and (c) overdrive. The two step settles in one half a period (~65X faster) and the overdrive in one third (~100X faster). The overdamped case are responses to (d) a normal step, (e) structured 500μs pulse, and (f) structured 100μs pulse. A 500μs settling time (~10X faster) requires 2.6X voltage overhead, and 100μs (~50X faster), requires 10.8X overhead.

IV. DC MAGNETIC FIELDS, OVERDAMPED CIRCUIT

In this section we discuss driving DC magnetic fields where the system is overdamped. Using the circuit shown earlier (Fig. 1), we now adjust the resistance and capacitance from underdamped to overdamped (Table 1). In this situation, the system is heavily overdamped. The simulated response to a square wave input is shown (Fig. 2d). This is the normal inductive response to a step input, which can be described as

$$I(t) = \frac{V}{R}\left(1 - e^{-\frac{R}{L}t}\right) \tag{3a}$$

where R is the series resistance, L is the inductance and t is the time after the step. For this set of values, the response time is >5ms. One can improve the settling time by using a structured drive signal. Drives with similar shape are implemented to achieve 500 µs (Fig. 2e) and 100 µs (Fig. 2f) settling times. These correspond to 10- and 50-fold improvement in settling time, compared to the step.

The engineered drive is constructed in the following way. There is a leading and trailing pulse added to the pulse that drives the system where we wish it to go. The width of those pulses is the desired transition time. In the simulations, pulse widths of 500 µs (Fig. 2e) and 100 µs (Fig. 2f) are used. The height of the pulses is calculated using Eq (3a) above. One uses the values of the inductance and resistance and plugs in the desired transition time into the equation.

$$V_{pulse}(T_{width}) = \frac{I_{final}R}{1-e^{\left(-\frac{R}{L}T_{width}\right)}} \tag{3b}$$

where I_{final} is the target current and T_{width} is the time wished to reach it. Here, we rely on the assumption that the system is linear.

The response to a normal step eventually plateaus at a final value (Fig. 2d). The relationship in Eq (3b) enables design of a pulse, which would achieve the same plateau value in a desired transition time. This can be used to calculate the height of the pulse for both initiating and terminating a response. For example, an engineered pulse for a desired transition time of 500 µs is 2.6022 times the plateau value (Fig. 2e). Comparatively, the response to a normal step after 500 µs, would be at 0.3843 of its final position (Fig. 2d). Similarly, a desired transition time of 100 µs yields a pulse height of 10.818 times the plateau value (Fig. 2f), while a normal step input would be at .09243 of its desired final position (Fig. 2d). One can use this algorithm to drive a DC field as quickly as one wishes, only limited by the voltage overhead available in the relevant electronics. It is noteworthy that, while the high voltage is applied to the inductive system, the current never exceeds the desired final value.

A useful rule of thumb can be obtained by examining a Taylor expansion of the exponential in Eq (3). This yields

$$V_{pulse} \sim L\frac{I_{final}}{T_{width}} \tag{4}$$

where V_{pulse} is the initial pulse height, T_{width} the initial pulse width, I_{final} is the current flowing through the system after it has settled down and L is the coil inductance. While not exact, this expression lets one initially configure a system and typically is within a few percent of optimal. This makes clear the relationship between the maximum driving voltage available and the minimum transition time achievable for any given equilibrium value of current. This expression should remind one of the relation $V = L\frac{dI}{dt}$ for inductors.

V. AC MAGNETIC FIELDS, UNDERDAMPED CIRCUIT

In this section, we discuss generating AC magnetic fields. In our circuit (Fig. 1), we again use the underdamped case values (Table 1). The simulated response of such an underdamped (high-Q) system is shown for an RF pulse intending to generate AC fields (Fig. 3a). The rise and fall time demonstrate the usual challenge in turning AC (RF) magnetic fields on and off quickly [4-11]. It takes many periods for the system to ring up when the drive voltage is applied and many periods to ring down when it is removed. The Q sets the response time, similarly to DC systems, this response can be controlled using an engineered drive (Fig. 3b and c). A simple case using a pulse and sine wave is demonstrated first (Fig. 3b). A DC pulse, one half a period in width, is used to start the system and then RF energy is fed into the system to counter the finite-Q. The timing is important. The starting pulse must be one half a period and the AC needs to be at the resonant frequency of the circuit and at the phase shown. One uses the DC pulse to "kick" the system and make it ring at its resonant frequency and then feeds in enough AC energy to counteract the losses in the system due to the finite-Q. Sine wave pumping is shown here but one can also use unipolar square waves, at the same phase as shown.

This expression for the initial and final pulses is derived from the exact solution to the relevant differential equation. The exact solution, for a sine pulse and sine drive, valid for all Q's is:

$$F = \frac{QA_{ac}}{c_1 e^{\alpha_1 \pi} + c_2 e^{\alpha_2 \pi} - Q\cos(\pi)} \tag{5}$$

where:

$$\alpha_1 = \frac{1}{2}\left(-\sqrt{\frac{1}{Q^2} - 4} - \frac{1}{Q}\right)$$

$$\alpha_2 = \frac{1}{2}\left(+\sqrt{\frac{1}{Q^2} - 4} - \frac{1}{Q}\right)$$

$$c_1 = \frac{Q\alpha_2}{\alpha_2 - \alpha_1} \qquad c_2 = Q - c_1$$

This expression is obtained by solving:

$$\frac{d^2y(t)}{dt^2} + \frac{1}{Q}\frac{dy(t)}{dt} + y(t) = \sin(t) \tag{6}$$

whose solution is:

$$y(t) = c_1 e^{\alpha_1 t} + c_2 e^{\alpha_2 t} - Q\cos(t) \tag{7}$$

where the constants are defined above (LC as well as V are set to unity). The integration constants, c_1 and c_2, are chosen so that $y'(0)=y(0)=0$. The solution is evaluated at the first peak, $t=\pi$, and this is used to scale the first drive pulse so that the amplitude is equal to the amplitude after the transients have decayed, QA_{ac}. In the infinite-Q limit, this goes to $2QA_{ac}/\pi$. In the high-Q limit, the initial, starting pulse is equal to the final, stopping pulse. However, for finite-Q, this is no longer true. Due to the finite losses, there is energy lost each cycle. The first pulse must be larger than the infinite-Q limit value to provide the energy lost in the first cycle and the final pulse is less by this same amount because energy is lost in the final cycle, requiring less of an impulse to stop the system (1st order correction). The initial and final pulse heights for sine pulse, sine wave driving and for square wave pulse, unipolar square wave driving are given (in the high-Q limit) by:

$$F_{Initial-sin} = \frac{2}{\pi}\left(1 + \frac{\pi}{4Q}\right) Q A_{ac} \tag{8}$$

$$F_{Final-sin} = \frac{2}{\pi}\left(1 - \frac{\pi}{4Q}\right) Q A_{ac} \tag{9}$$

$$F_{Initial-sq} = \frac{1}{2}\left(1 + \frac{\pi}{4Q}\right) Q A_{ac} \tag{10}$$

$$F_{Final-sq} = \frac{1}{2}\left(1 - \frac{\pi}{4Q}\right) Q A_{ac} \tag{11}$$

Approximations for Eqs (8)-(11) are shown (Fig. 3g) for sine and square wave driving, as well as the exact solution, Eq. (7), for the sine leading pulse. Notably, the approximations work very well for Q>10. Here, we have normalized the Q dependence in Eqs. (8)-(11). As one usually has a finite amount of voltage overhead to work with in the drive electronics, a DC

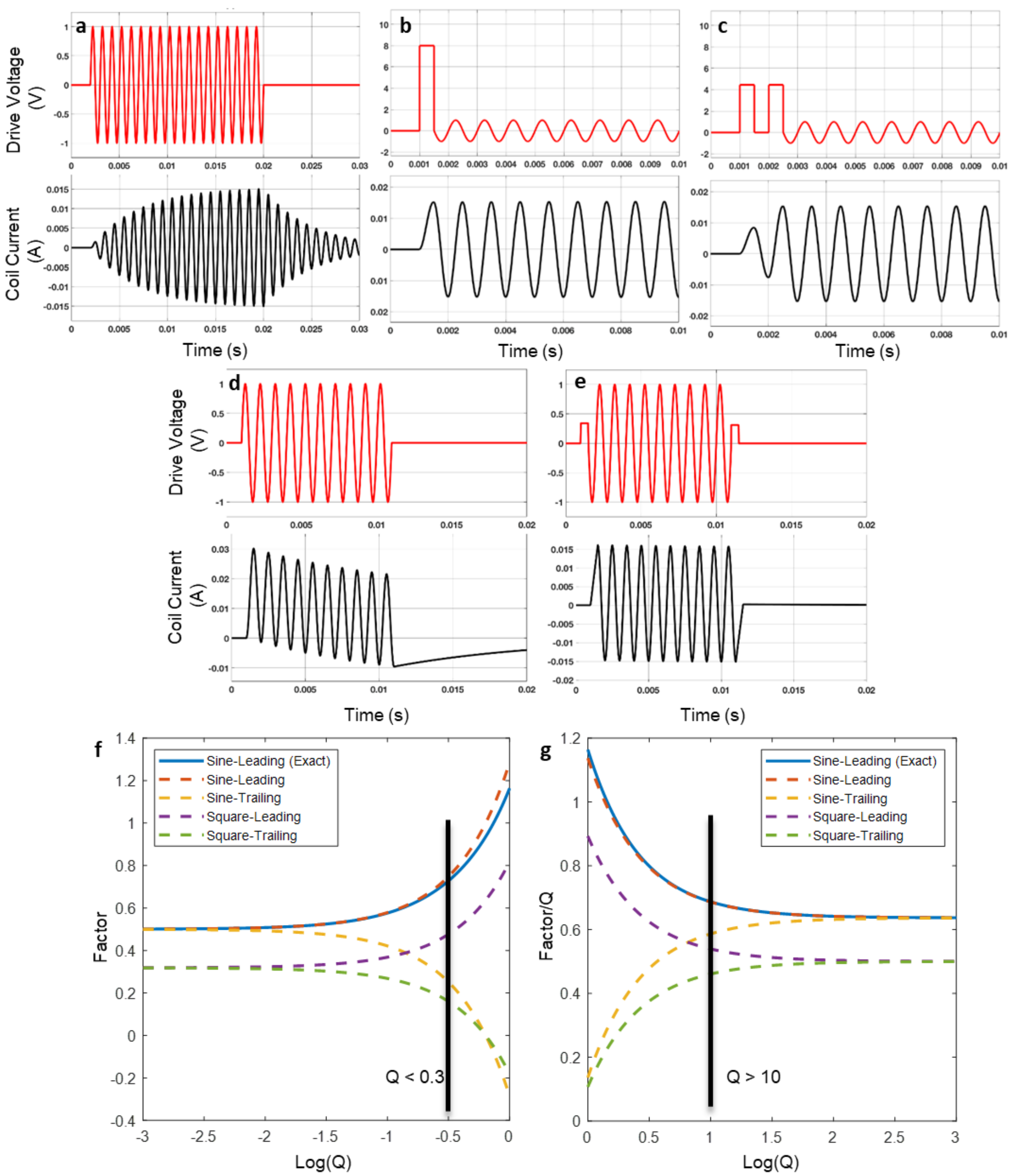

Fig. 3. AC Magnetic Field Simulations and Q-Limits in Drive Design. Shown (a-e) are Simscape simulations of the parallel LCR circuit shown in Fig. 1, for underdamped (a-c) and overdamped (d and e) parameters in Table 1 and an AC drive (voltage drives are red/top and the inductor currents are black/bottom. The underdamped case are responses to (a) a normal RF pulse, (b) a single DC pulse with sine wave pumping, and (c) two smaller DC pulses with sine wave pumping. The single pulse settles in half a period (~35X faster). Depending on system requirements, this can be done with multiple smaller pulses (c) or with PWM (Fig. S1). The overdamped case are responses to (d) a normal RF pulse and (e) a single DC pulse with sine wave pumping. Q-limits in designing AC drives for faster ring up and ring down are shown for overdamped (low-Q) (f) and underdamped (high-Q) (g) for multiple pulse shapes, based on analytical solutions.

initial pulse is preferable because the power factor is 1 for a square pulse but only 0.707 for a sine pulse, requiring a larger voltage excursion for the same impulse. This is the AC equivalent of the two-step drive discussed earlier where one puts the energy into the AC mode in two steps to get the system started in a bipolar way. The square/square unipolar is interesting because one can implement it with a fast switch and a fixed DC voltage using pulse width modulation (PWM) to adjust the differing driving forces (Fig. S1). In this case, Eq. (5) would represent the ratio of duty cycles instead of amplitudes. Typically, the PWM frequency would need to be at least 100 times the system resonant frequency.

The basic approach for AC magnetic drive is that one feeds in energy at the resonant frequency to counteract the losses and this energy must be fed in phase, coherently to the system. If a large starting pulse is inconvenient (Fig. 3b), one can use two or more starting pulses (Fig. 3c), each a fraction of the single pulse. It is important that they be applied coherently to the system. A single large pulse is replaced by two pulses, each roughly one half the single larger pulse, applied on for half a period, off for half a period, on for half a period, off for half a period, etc., until the sine wave drive is applied. If the starting DC pulse is applied as a single pulse, the system turns on and off in less than a single period of the system (Fig. 3b). If more than one starting or stopping pulse is used, it takes several periods to ring up (Fig. 3c). However, this is always faster than using a simple RF pulse. Two starting pulses ring the system up in roughly a full period of the system while the standard RF drive takes tens of periods of the system to reach equilibrium.

A key point to note is that the conventional drive responds more slowly for higher Q, while our approach actually responds faster the higher Q is. With one starting DC pulse, the system responds in less than a period for a Q of ten or ten thousand. As discussed earlier, this has great application for NMR systems, which is also shown later in Section VIII. The key point is that the pulse used to turn off the pulse train needs to be phase coherent with the underlying system dynamics. To create this drive, we offer the following empirical approach. Start with the initial AC voltage one wishes to apply. Then use Eqs (8)-(11) to calculate the height of the initial and final pulses. The width needs to be half a period of the system to be driven. If the Q is less than 10, the exact solution, Eq (5), may be needed.

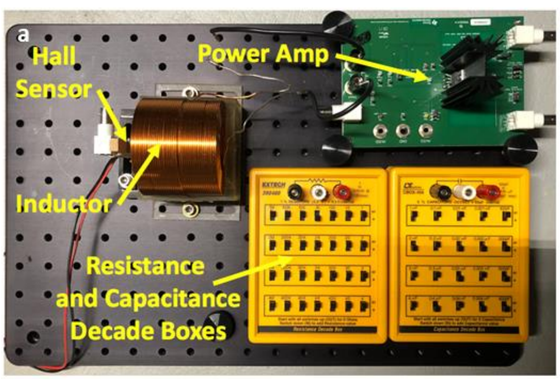

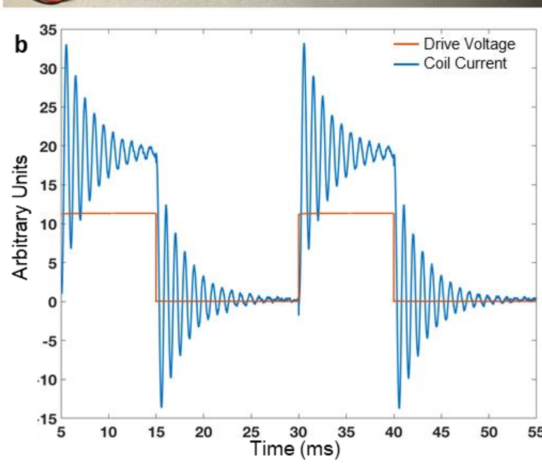

Fig. 4. Experimental Testbed. (a) A high-Q inductor with an adjustable LCR circuit has (b) a typical step-and-settle response without a structured drive.

VI. AC Magnetic Fields, Overdamped Circuit

In this section, we discuss the overdamped AC drive. In the circuit (Fig. 1), we use overdamped values (Table 1). Simulations of the conventional system (Fig. 3d) and the engineered drive (Fig. 3e) are presented. In the conventional drive, the input and output are asymmetric and do not start and stop in a convenient place. Using small DC pulses, one can optimize the response. Conventionally, applying a positive pulse produces a unipolar response and then relaxes during the pulse train to a bipolar response (Fig. 3d). In the overdamped limit, Eq (5) also works. For high-Q systems, the amplitude of the initial DC pulse is greater than the AC amplitude, but it is less in the overdamped case (Fig. 3e). The expression (5) works for Q>1 and also Q<1. This is the AC equivalent of the two-step drive discussed earlier where one puts the energy into the AC mode in two steps to get the system started in a bipolar way. It is convenient that formula (5) works for any value of Q (Fig. 3f and g). The low-Q approximations to Eq (5) are given below.

$$F_{Initial-sin} = \frac{1}{2}\left(1 + \frac{\pi Q}{2}\right) A_{ac} \tag{12}$$

$$F_{Final-sin} = \frac{1}{2}\left(1 - \frac{\pi Q}{2}\right) A_{ac} \tag{13}$$

$$F_{Initial-sq} = \frac{1}{\pi}\left(1 + \frac{\pi Q}{2}\right) A_{ac} \tag{14}$$

$$F_{Initial-sq} = \frac{1}{\pi}\left(1 - \frac{\pi Q}{2}\right) A_{ac} \tag{15}$$

These low-Q approximations are compared (Fig. 3f), where the exact solution from Eq (5) is included. The approximations in Eqs (12)-(15) work well for Q<0.3, as can be observed graphically where the approximation follows the exact solution in the sine-leading case.

VII. Experimental Results on an LCR System

To demonstrate the operation of our algorithms in all four cases, we developed an experimental testbed (Fig. 4a). It consists of a high-Q inductor with inductance of 10.31 mH and a coil resistance of 1.16 Ω. We sense the DC and AC magnetic fields using a Hall sensor (Allegro A1232). The bandwidth of the sensor is 30 kHz with a sensitivity of 2.5 mV/Gauss. We are using a power amplifier based on the Texas Instruments OPA 548 op-amp. It has a gain bandwidth product of 1 MHz. We used a combination of multiplier and summer circuits to construct the various drive waveforms and the signals were

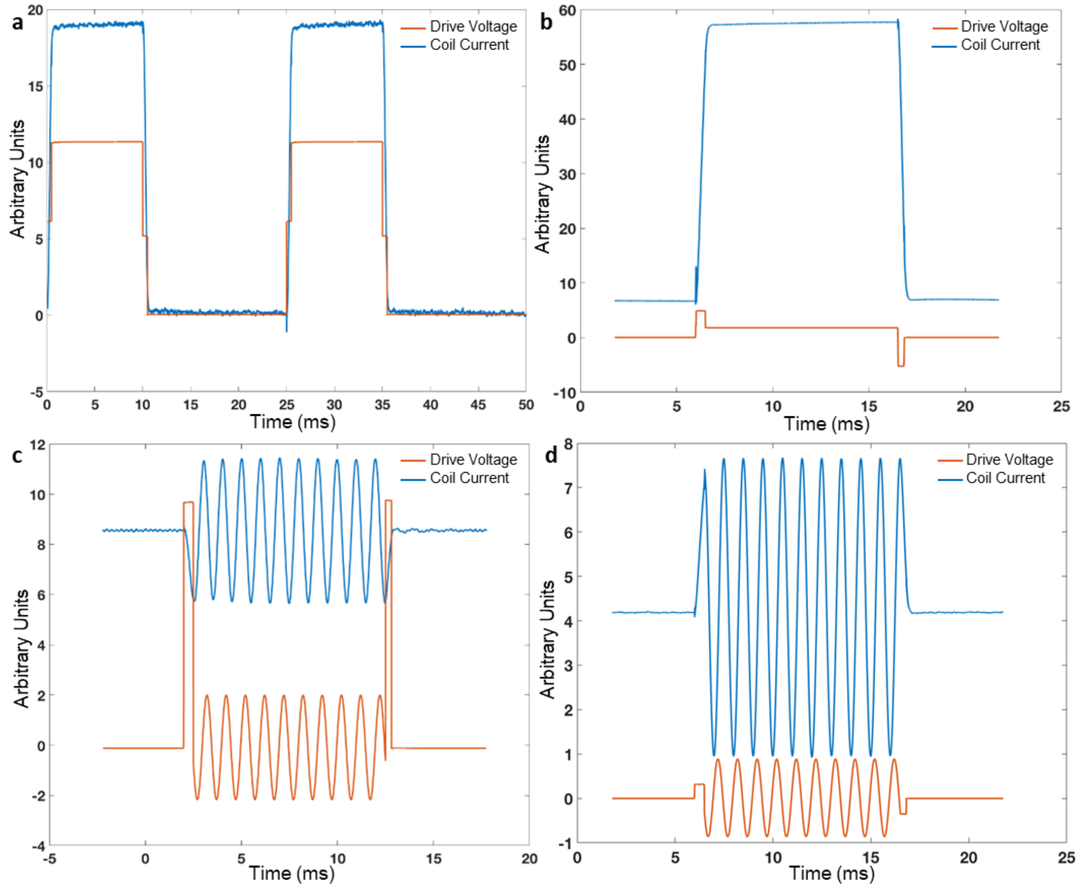

Fig. 5. Experimental Results with Structured Drives. Here, (a) and (c) are underdamped, while (b) and (d) are overdamped. Engineered DC drives are demonstrated in (a) and (b), and engineered AC drives are drives are shown in (c) and (d).

captured and digitized on an oscilloscope. The setup (Fig. 4a) is constructed specifically so that decade boxes are adjusted to match the system parameters in Table 1 for the both underdamped and overdamped cases. For experimental data (Fig. 4b and Fig. 5), we use a voltage drive. We also demonstrate experimental data for a current drive (Fig. S2).

We demonstrate our algorithms in operation on a real system in Fig. 5. The typical step response for the DC underdamped case displays a long settling time observed by ringing (Fig. 4b). We optimize settling in this case (Fig. 5a) by applying the two-step drive as discussed earlier (Fig. 2b). In the drive, we apply half of the force for half a period (500 μs). After the half period, we apply the full force. As one can see, the drive algorithm improves the step-and-settle time by a factor of more than 20.

We also demonstrate application of our algorithms in the other three cases: DC overdamped (Fig. 5b), AC underdamped (Fig. 5c), and AC overdamped (Fig. 5d). One starts the oscillating mode with the initial DC pulse, counteracts the losses in the system by feeding in AC drive at the resonant frequency and then turns the mode off with a final pulse. The experimental results demonstrate the same behavior seen in both the Simscape simulation (Fig. 2 and 3) and the Simulink s-space simulation (Fig. S3).

VIII. NMR Application

Nuclear magnetic resonance (NMR) is an example where producing short RF pulses presents a challenge [4]-[11], [18]-[23]. The inset of Fig. 6a shows a typical NMR circuit. The nuclear spins under study are located inside an inductor L whose effective RF resistance is represented by R (typically a few Ohms and weakly frequency dependent). The frequency of operation, also known as the Larmor frequency, is $\omega = \gamma_n B_0$ where B_0 is the static applied magnetic field and γ_n is the gyromagnetic ratio of the nucleus under study. In the simplest case, there are two steps required to obtain an NMR signal. First, a tone burst of duration τ is applied at the Larmor frequency, generating a large RF magnetic field B_1 inside the coil. This field forces the nuclear spin magnetization to rotate away from its equilibrium direction by an angle $\varphi = \gamma_n B_1 \tau$. For maximum signal, one often chooses τ (typically microseconds) so that $\varphi = 90$ degrees. Once the RF tone burst ends, the nuclear spin magnetic moment is out of equilibrium. It precesses at the Larmor frequency, causing a changing magnetic flux through the coil and a signal voltage via Faraday's Law. The signal is called a free induction decay (FID) and is typically microvolts to millivolts in magnitude, persisting microseconds to many milliseconds depending on nuclear spin-spin relaxation time and the magnet homogeneity [21]. Both processes, transient RF field generation and signal detection are improved by using a high-Q coil in a resonant circuit.

It is generally advantageous to make B_1 as large as possible to ensure that other nuclear spin interactions are negligible compared to their interaction with B_1. For this reason, the resonant circuit must also be impedance matched to the power amplifier and transmission line (typically 50 Ohm). For many situations, a constant amplitude B_1 waveform (a so-called hard pulse) is desired but in other cases it is desirable to shape the

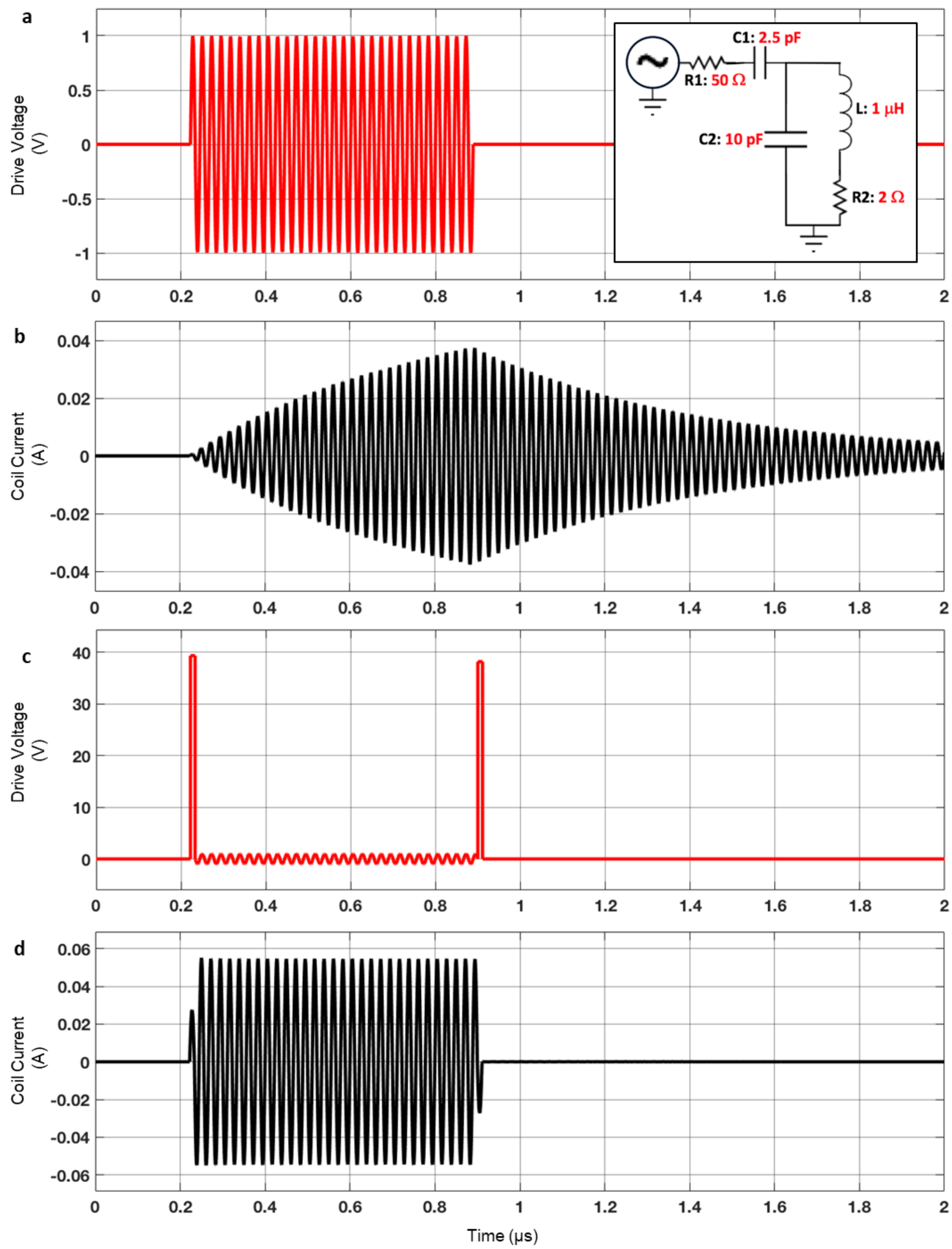

Fig. 6. Simulation Results with a Typical NMR Circuit. The circuit (a inset) has a resonance of 45 MHz and a Q of 141. A typical RF pulse (a) is imposed on the circuit, producing long ring up and ring down times of ~10μs (b). An engineered drive (c) developed from our algorithms yields much faster AC settling, with ring down and ring up times of ~10ns, or half a period.

waveform to tailor its Fourier spectrum. The latter is used extensively in MRI to excite spins in a particular spatial slice. In any case one wants to tailor the B_1 waveform but minimize the excessive rise and fall times associated with a high quality factor resonant circuit. The decay time is particularly problematic in low frequency applications of magnetic resonance since the ringdown time of the resonant circuit $\tau_Q = 2Q_L/\omega$. Here, Q_L is the loaded Q which, under impedance matched conditions, is ½ the unloaded Q of the isolated tank circuit. This problem has typically been addressed with active Q-suppression circuits [22]-[23] which add complexity and only partially mitigate the problem.

The circuit shown in Fig. 6a inset is widely used in NMR to generate large RF currents through the coil. Capacitors C_1 and C_2 are required to tune and match the inductor to a power amplifier and transmission line. The capacitors also provide an impedance match to the receiving circuit (not shown). The component values were chosen to tune and match to a Q = 141 coil to 50 Ohms at 45 MHz. Fig. 6a shows The voltage waveform applied to the amplifier is a constant amplitude RF pulse of duration ~0.6 μs (Fig. 6a). The resulting coil current

(Fig. 6b) first rises and then rings for a long time after the RF pulse is applied.

The decaying tail of the pulse can be particularly problematic since one wishes to begin detection of the FID as soon as possible after the end of the RF pulse. Since the coil ringdown voltage may start out orders of magnitude larger than the FID, there is considerable dead time, sometimes as much as $20\tau_Q$, after the pulse ends before it is possible to begin recording the FID. This dead time introduces phase errors, complicates the transformation of the FID into a spectrum, and significantly reduces the available signal to noise ratio [23]. The problem is typically solved by using spin echoes, which are widely separated from the RF pulse but there are times when an FID is needed. Coil ringing may also place a lower limit on the pulse spacing in multiple pulse sequences. In these cases, Q-suppression methods may be required. Since the signal to noise ratio of the NMR signal is typically proportional to $Q^{1/2}$, one is generally hesitant to sacrifice quality factor.

This problem may be solved with engineered drives (Fig. 6c and d). The drive voltage (Fig. 6c) is constructed using the same methods shown earlier for the AC underdamped circuit (Fig. 3b and 5c). One puts energy into the mode with a DC pulse, keeps energy in the mode with AC current and then dumps the mode with a final DC pulse. The next panel shows the voltage across the coil. The bottom panel shows the essential quantity, the coil current, which is proportional to the B_1 field. Both the coil voltage and coil current waveforms are extremely clean with transition times well less than a period. The difference between this response to an engineered drive (Fig. 6d) and the standard drive (Fig. 6b) is striking.

IX. Conclusion

In this paper we have presented a series of open loop control algorithms for achieving rapid step and settle response times in AC and DC inductive systems. In all four cases, DC and AC, over and underdamped, these algorithms allow one to rapidly turn the generated magnetic fields on and off quickly. Finally, we apply these techniques to a common inductor problem of driving NMR coils. This paper attempts to be a collection of tricks and techniques that will be useful to the scientist or engineer wishing to quickly start and stop DC and AC magnetic fields, not a theoretical treatise. As such, we hope the readers will find these methods useful.

Appendix

Supplementary information, including text and 4 figures is included in the *SI Appendix*.

Acknowledgment

The authors would like to thank Dr. Amy Freund, Senior Applications Scientist at Bruker Biospin for her helpful advice on high impact problems related to gold standard NMR techniques. This work was supported by the NSF CELL-MET ERC award no. 1647837.

References

[1] Imboden, Matthias, Jackson Chang, Corey Pollock, Evan Lowell, Mehmet Akbulut, Jessica Morrison, Thomas Stark, Thomas G. Bifano, and David J. Bishop. "High-speed control of electromechanical transduction: Advanced drive techniques for optimized step-and-settle response of MEMS micromirrors." IEEE Control Systems Magazine 36, no. 5 (2016): 48-76.

[2] Barrett, Lawrence, et al. "Modal Engineering for MEMS Devices: Application to Galvos and Scanners." (2020).

[3] Pollock, C., et al. "Extreme angle, tip-tilt MEMS micromirror enabling full hemispheric, quasi-static optical coverage." Optics express 27.11 (2019): 15318-15326.

[4] Du, Guanfeng, et al. "Study on Shortening the Dead Time of Surface Nuclear Magnetic Resonance Instrument Using Bipolar Phase Pulses." IEEE Transactions on Instrumentation and Measurement 69.4 (2019): 1268-1274.

[5] Marjanovic, Josip, et al. "Multi-rate acquisition for dead time reduction in magnetic resonance receivers: Application to imaging with zero echo time." IEEE transactions on medical imaging 37.2 (2017): 408-416.

[6] Lin, Tingting, et al. "Exploring on the sensitivity changes of the LC resonance magnetic sensors affected by superposed ringing signals." Sensors 18.5 (2018): 1335.

[7] Prabhu Gaunkar, N., et al. "Analysis of ringing effects due to magnetic core materials in pulsed nuclear magnetic resonance circuits." Journal of Applied Physics 117.17 (2015): 17E508.

[8] Gaunkar, NG Prabhu, et al. "Broadband analysis of response from magnetic cores used in inductive sensors for pulsed nuclear magnetic resonance applications." IEEE Transactions on Magnetics 52.7 (2016): 1-4.

[9] Amouzandeh, Ghoncheh, et al. "Time and Frequency Domain Response of HTS Resonators for Use as NMR Transmit Coils." IEEE Transactions on Applied Superconductivity 29.5 (2019): 1-5.

[10] Burghoff, M., et al. "SQUID systems adapted to record nuclear magnetism in low magnetic fields." IEEE Transactions on applied superconductivity 17.2 (2007): 846-849.

[11] Dong, Hui, et al. "Suppression of ringing in the tuned input circuit of a SQUID detector used in low-field NMR measurements." Superconductor science and technology 22.12 (2009): 125022.

[12] Wang, Wei, et al. "Relaxation behavior study of ultrasmall superparamagnetic iron oxide nanoparticles at ultralow and ultrahigh magnetic fields." The Journal of Physical Chemistry B 115.49 (2011): 14789-14793.

[13] Tu, Liang, et al. "Measurement of Brownian and Néel relaxation of magnetic nanoparticles by a mixing-frequency method." IEEE transactions on magnetics 49.1 (2012): 227-230.

[14] Javor, Josh, et al. "A Microtissue Platform to Simultaneously Actuate and Detect Mechanical Forces via Non-Contact Magnetic Approach." Journal of Microelectromechanical Systems (2020).

[15] Urasaki, Naomitsu, et al. "Adaptive dead-time compensation strategy for permanent magnet synchronous motor drive." IEEE Transactions on Energy Conversion 22.2 (2007): 271-280.

[16] Normey-Rico, Julio E., and Eduardo F. Camacho. "Robust tuning of dead-time compensators for processes with an integrator and long dead-time." IEEE Transactions on Automatic Control 44.8 (1999): 1597-1603.

[17] Pollock, Corey, Matthias Imboden, Alexander Stange, Josh Javor, Koshik Mahapatra, Leila Chiles, and David J. Bishop. "Engineered PWM drives for achieving rapid step and settle times for MEMS actuation." Journal of Microelectromechanical Systems 27, no. 3 (2018): 513-520.

[18] Yamada, Takeshi, et al. "Electromagnetic evaluation of HTS RF coils for nuclear magnetic resonance." IEEE Transactions on Applied Superconductivity 25.3 (2014): 1-4.

[19] Avadhut, Yamini S., Denis Schneider, and Jörn Schmedt auf der Günne. "A method for improved quantification of 1H NMR signals under low-resolution conditions for solids." Journal of Magnetic Resonance 201.1 (2009): 1-6.

[20] Dabaghyan, Mikayel, et al. "A portable single-sided magnet system for remote NMR measurements of pulmonary function." NMR in Biomedicine 27.12 (2014): 1479-1489.

[21] Webb, G. A. "CP Slichter. Principles of magnetic resonance. Springer series in Solid-State Sciences, Vol. by M. Cardoua, P. Fulde and HJ Queisser, Springer-Verlag, Berlin (1978). 397 pages. DM 54, US $27.00." Organic Magnetic Resonance 12.3 (1979): IV-IV.

[22] Conradi, Mark S. "FET Q switch for pulsed NMR." Review of Scientific Instruments 48.3 (1977): 359-361.

[23] Zhen, J. Z., et al. "A resistive Q-switch for low-field NMR systems." Journal of Magnetic Resonance 287 (2018): 33-40.